EPiC Series in Engineering
Volume 3, 2018, Pages 564–571
HIC 2018. 13th International Conference on Hydroinformatics

Numerical simulation of a dam-break wave propagating over an erodible floodplain in presence of a structure

Cristiana Di Cristo[1], Massimo Greco[2], Michele Iervolino[3,*] and Andrea Vacca[2]

[1] Università di Cassino e del Lazio Meridionale via G. Di Biasio 43, Cassino (FR) 03043, Italy
[2] Università di Napoli 'Federico II' via Claudio 21, Napoli 80125, Italy
[3] Università della Campania 'Luigi Vanvitelli' via Roma 9, Aversa (CE) 81031, Italy
dicristo@unicas.it, grecom@unina.it,
michele.iervolino@unicampania.it, vacca@unina.it

Abstract

Climate change is exposing more and more frequently flood prone areas to potential casualties and damages. The capability of the flow to carry relevant quantities of sediments interacts with the presence of obstacles in flood-inundated areas and contributes to the increase the related hazard, constituting a relevant concern in the framework of risk analysis. Unfortunately, existing literature on this topic is rather scarce, especially for the features of sediment transport and the forces acting on rigid obstacles. In the paper, a recent two-phase shallow-water morphodynamical model, particularly suited to the analysis of fast geomorphic transients, is applied to the numerical simulation of the propagation of a dam-break wave over an erodible floodplain in presence of a rigid obstacle. The geometry of the test-case is inspired to a recent fixed-bed study reported in the literature, for which extensive experimental and numerical data concerning the flow field and the dynamic loading against the obstacle are available. Results of the numerical simulations contribute to highlight the effect of the obstacle on the changes in the bottom topography, along with the subsequent change on the loading condition on it.

* Corresponding author

G. La Loggia, G. Freni, V. Puleo and M. De Marchis (eds.), HIC 2018 (EPiC Series in Engineering, vol. 3), pp. 564–571

1 Introduction

The magnitude of floods caused by intense rainfall is becoming more and more severe because of climate change [1]. In turn, the exposition of initially dry areas to flood waves arising from the failure of embankments or dikes has increased.

The interaction between the capability of the flood to carry relevant quantities of sediments and the presence of obstacles (for instance buildings, piles) in the inundated areas both contribute to affect the flood wave propagation. On one hand, the obstacles deviate the flow pattern and the morphological change induced by the flow may expose the obstacle to unexpected loading condition, contributing therefore to its structural damage. For these reasons, the propagation of flood waves over loose sediment bed and its interaction with the obstacles constitute a relevant concern in the framework of risk analysis.

Accounting for the results of several studies concerning flows over non-erodible beds, the shallow-water formulation can be considered a reasonable approach for the simulation of these complex processes, especially if the attention is focused on mid- and far-field effects. For example, [2] investigated a two-dimensional (2D) flood flows and the hydrodynamic force acting on structures, showing that the prediction accuracy of the shallow-water model is acceptable for both hydrodynamics and force evaluation. Successfully, [3] applied a shallow-water model to predict the dynamic action exerted by a dam-break wave on a vertical wall.

The potentiality of a depth-averaged shallow-water model in reproducing the propagation in urban areas of both flash floods and dam-break waves has been investigated in [4] and in [5]. Numerical results, in terms of both flow depths and velocities, fairly agree with experimental ones, although some discrepancies were observed around buildings, where the flow is strongly 3-D. More recently, [6] compared the predictions of a 2D depth-averaged model, a 3D Eulerian two-phase model and a 3D Smoothed Particle Hydrodynamics (SPH) model, in the simulation of the forces exerted by a dam-break wave on a rigid squat structure. Comparing the numerical and the experimental results, the Authors found that the error in the peak load for the 2D model based on the shallow-water approach was in the order of 10%.

As far as the simultaneous presence of obstacles and of an erodible floodplain is concerned, the literature is less rich. From the experimental point of view, the tests by [7] and the test-cases studied under the NSF-Pire project [8], concerning a dam-break in an erodible channel with a sudden enlargement, contributed to shed some light on the basic elements of the interaction of the flood wave with rigid walls. However, they neither considered any obstacle in the floodplain nor evaluated the impact forces.

The numerical analyses which have been subsequently developed support the idea that also for this kind of processes, the shallow-water approximation represents a suitable framework, provided that an adequate modelling of the non-equilibrium sediment transport is accounted for. To match this requirement, several non-equilibrium models have been proposed, which can be grouped into mixture single-layer (e.g. [9]), multi-layer (e.g., [10, 11, 12, 13]) or multi-phase (e.g. [14, 15, 16, 17]).

In the present paper, a numerical study of the propagation of a dam-break wave over an erodible floodplain in presence of a rigid obstacle is carried out. To this aim, the shallow-water two-phase model by [17] is used for reproducing the same geometry of the fixed-bed test case by [6].

2 Material and methods

In what follows, the considered test-case is described, along with the morphodynamical model adopted for numerical simulations.

2.1 The considered test-case

Figure 1 depicts the reproduction of the plan view of the test-case by [6].

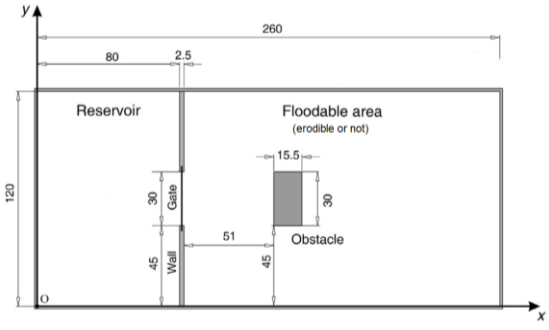

Figure 1: Sketch of the considered test-case (dimensions are in centimeters).

The flow originates from the sudden removal of the gate, which induces the propagation of a dam-break wave over the floodable area. In the first simulation, the latter is assumed to be non-erodible, thus reproducing the same layout investigated by [6]. In a second series of simulations, the floodplain is assumed to be constituted by a loose sediment with variable properties ranging from fine sand to coarse sand.

2.2 The mathematical model

A brief description of the model presented in [17] is provided below, whereas the reader is referred to the original reference for further details about model assumptions and limitations, as well as for the method employed for the numerical simulation. Since, in the present application the suspended load has been neglected, the model consists of equations expressing the mass and momentum conservation for the liquid (Eqs. 1 and 3) and the solid phase as bed load (Eqs. 2 and 4). Finally, Eq. (5) predicts the bed deformation. They read:

$$\frac{\partial \delta_l}{\partial t} + \nabla \cdot \left(\delta_l \mathbf{U}_l\right) - p e_B = 0 \tag{1}$$

$$\frac{\partial \delta_{s,b}}{\partial t} + \nabla \cdot \left(\delta_{s,b} \mathbf{U}_s\right) - \left(1-p\right) e_B = 0 \tag{2}$$

$$\frac{\partial \delta_l \mathbf{U}_l}{\partial t} + \nabla \cdot \left(\delta_l \mathbf{U}_l \mathbf{U}_l\right) + \nabla\left(\frac{g h^2}{2}\right) + g h \nabla\left(z_B\right) + \mathbf{S}_l = 0 \tag{3}$$

$$\frac{\partial \delta_{s,b} \mathbf{U}_s}{\partial t} + \nabla \cdot \left(\delta_{s,b} \mathbf{U}_s \mathbf{U}_s\right) + \frac{r}{r+1} \nabla\left(\frac{g \delta_{s,b}^{\,2}}{2 C_{s,b}}\right) + g \delta_{s,b} \frac{r}{r+1} \nabla\left(z_B\right) + \mathbf{S}_s = 0 \tag{4}$$

$$\frac{\partial z_B}{\partial t} + e_B = 0 \tag{5}$$

in which t is the time, g is the gravity acceleration, $r = (\rho_s - \rho_l)/\rho_l$ with ρ_l and ρ_s constant liquid and solid densities, respectively. δ_l denotes the liquid phase volume for unit bottom surface and $\delta_{s,b}$ is the solid phase volume transported as bed load for unit bottom surface. Hence, denoting by z_w and z_B, respectively, the free surface and bottom elevation, $h = z_w - z_B = \delta_l + \delta_{s,b}$. $\mathbf{U}$ is the phase-averaged velocity vector, with the subscript l and s denoting the water and the solid phase, respectively. For both phases, the second-order tensor $\mathbf{UU}$ denotes the diadic product of the phase-averaged velocity with itself. $C_{s,b}$ is the bed load volume concentration and e_B is the bottom erosion/deposition rate.

The source terms of momentum equations S_l and S_s are given by:

$$\mathbf{S}_l = \frac{\mathbf{U}_l}{C_{\mathrm{Ch}}^2}\left|\mathbf{U}_l\right| - (r+1)\mu_d g \delta_{s,b}\frac{r}{r+1}\frac{\mathbf{U}_s}{\left|\mathbf{U}_s\right|} - \alpha(r+1)\mathbf{U}_s\left|\mathbf{U}_s\right| + g\delta_{s,b}s_B + \frac{\mathbf{D}}{\rho_l} \tag{6}$$

$$\mathbf{S}_s = \mu_d g \delta_{s,b}\frac{r}{r+1}\frac{\mathbf{U}_s}{\left|\mathbf{U}_s\right|} + \alpha\mathbf{U}_s\left|\mathbf{U}_s\right| - \frac{\mathbf{D}}{\rho_l} \tag{7}$$

where μ_d is the dynamic friction coefficient, C_{Ch} is the dimensionless Chezy coefficient, s_B is the bottom slope, **D** is the drag force of the liquid on the solid particle, and α is the collisional stress coefficient. In Eq. (7), the first two terms represent the ratio $\tau_{B,s}/\rho_s$, where the bottom shear stress, attrition, particle collision and drag exchange between liquid and solid phase $\tau_{B,s}$ accounts for both frictional and inter-particles collisional stresses. In Eq. (6), the first four terms represent the ratio $\tau_{B,l}/\rho_l$, where the bottom shear stress on the liquid phase, $\tau_{B,l}$, is expressed as the difference between the shear stress which would act upon the bottom in the absence of sediment transport and the momentum transferred to the solid phase $\tau_{B,s}$. The drag force **D** is evaluated as:

$$\mathbf{D} = \rho_l C_D \frac{\delta_{s,b}}{d}\left(\mathbf{U}_l - \mathbf{U}_s\right)\left|\mathbf{U}_l - \mathbf{U}_s\right| \tag{8}$$

where C_D is a bulk drag coefficient and d is the sediment particle diameter. The bottom entrainment/deposition is expressed through the following formula [18]:

$$e_B = w_s\frac{T^{3/2} - C_{s,b}}{1-p} \tag{9}$$

in which w_s denotes the sediment settling velocity, computed as a function of $C_{s,b}$ using the semi-empirical formula by [19]. The dimensionless mobility parameter T, which accounts for the excess of the mobilizing stresses onto the bottom surface with respect to the resisting ones [20], is evaluated through the following formula:

$$T = \frac{\left|\boldsymbol{\tau}_{B,l} + \boldsymbol{\tau}_{B,s} - \boldsymbol{\tau}_c - \boldsymbol{\tau}_B\right|}{\left|\boldsymbol{\tau}_c + \boldsymbol{\tau}_B\right|} \tag{10}$$

where $\boldsymbol{\tau}_c$ is the threshold shear stress for sediment motion and $\boldsymbol{\tau}_B$ is the magnitude of Mohr-Coulomb stress at the bottom, with μ_s the static friction coefficient. Even if the coefficient α and C_D could be estimated from existing empirical formulas, their expression has been deduced based on the analysis of uniform flow conditions [17], obtaining the following relations:

$$\alpha = \frac{(1-c_1) - k_1(\mu_d - s_B)}{(r+1)k_2^{\,2}}, \quad C_D = \frac{1-c_1}{k_1}\frac{\rho_l g d r}{\left[C_{\mathrm{Ch}}\tau_0^{\,1/2} - k_2(\tau_0 - \tau_c)^{1/2}\right]^2} \tag{11}$$

where k_1 and k_2 are the following two dimensionless coefficients:

$$k_1 = \frac{1}{2\mu_s}\frac{2+(1-p)^{2/3}}{1+(1-p)^{2/3}}, \quad k_2 = \frac{K_{MPM}}{k_1} \tag{13}$$

In eq. (13), KMPM is the Meyer-Peter and Müller formula coefficient and c_1 is a dimensionless model parameter. With the above closures, the model application requires the definition of only three independent dimensionless parameters. Two of them, characterizing the shear stress, C_{Ch} and K_{MPM}, may be evaluated from standard literature. The remaining free model parameter c1, it is bounded between the lower and upper limits theoretically deduced, with a reduced sensitivity of the results to its variation [17].

The system of Eqs. (1)-(5), which is shown to be hyperbolic [17], is solved with a code using 2D unstructured quadrilateral meshes. The numerical method relies on a mixed cell-centred (CCFV) and node-centred (NCFV) finite-volume discretization. The former is adopted for the variables δ_l, $\delta_{s,b}$,$\mathbf{U}_l$ and $\mathbf{U}s$, defined at the grid cell centres, the latter for the bed elevation z_B, with the control volumes constructed around the mesh nodes by the median-dual partition [21, 22]. The numerical fluxes in the

CCFV discretization of Eqs. (1)-(4) are calculated through the first-order Harten–Lax–Van Leer (HLL) scheme [23], with second-order reconstruction of free surface level for subcritical flow [24].

3 Results and discussion

The model discussed in the previous section has been applied to the numerical simulation of the problem sketched in Figure 1. In the first simulation, the floodplain is assumed to be non-erodible, thus reproducing the same case investigated by [6]. In a second series of simulations, the floodplain is assumed to be constituted by a loose sediment. Two scenarios have been considered, by changing the sediment diameter from $5 \cdot 10^{-4}$ m, representative of a fine sand, to $5 \cdot 10^{-3}$ m, which is typical of a coarse sand. In all the simulations, C_{Ch}=12 and a mesh with Δx=Δy=$5 \cdot 10^{-3}$ m are adopted, along with Δt=1/1024 s. Moreover, based on the simulated flow fields, the time history of the impact force on the downstream obstacle has been evaluated.

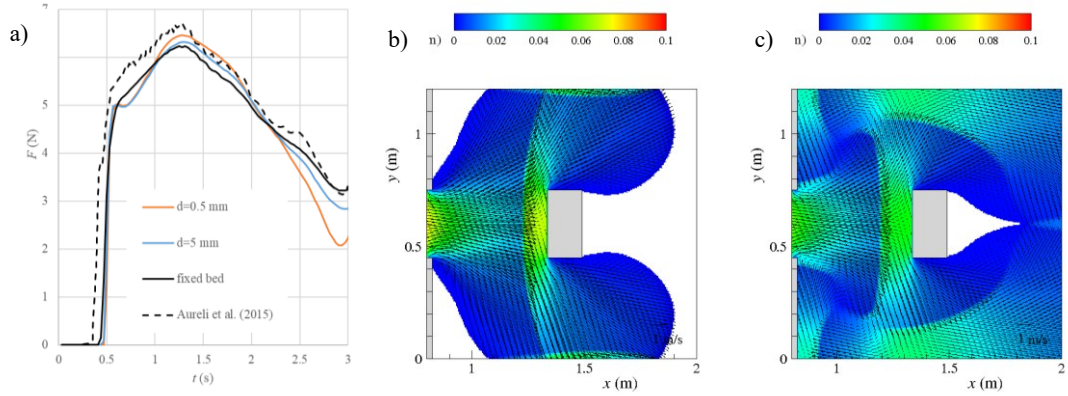

Figure 2: a) Time history of the impact forces over the downstream obstacle for fixed and mobile bed cases; Contour level of the free-surface elevation and velocity vector plot over fixed bed b) at t = 1.25 s; c) at t = 3.0 s.

Figure 2a shows the time history of the impact force F on the downstream obstacle for the fixed and mobile bed cases and Figure 2b and 2c report the contour levels of the free-surface elevation and the velocity vector plot at t = 1.25 s and t = 3.0 s for the fixed bed case, respectively.

As far are the non-erodible case is concerned, the results essentially agree with those from the shallow-water model of [6]. After the impact of the wave on the obstacle (t ~ 0.5 s), an abrupt increase of the force is observed, which reaches its maximum value (F ~ 6 N) at t ~ 1.25 s (the corresponding flow field is reported in Fig. 2 b), and then it quasi-monotonically decreases, reaching half of the peak value at t ~ 3.0 s, whenever the flood wave completely surrounds the obstacle (Fig. 2 c). Bottom mobility only marginally influences the load dynamics on the obstacle, especially in the first instants. The time at which the impact and the peak force occur, along with the peak force, only slightly depend on the sediment composing the mobile bottom.

This conclusion is supported by the examination of the local characteristics of the flow field. Figure 3 compares, the free-surface elevation (with the velocity vector field superposed), the bottom topography and the flow momentum at t = 1.25 s, for the finest (Fig. 3a-c) and the coarsest sediments (Fig. 3d-f). Independently of the bottom material dimensions, Figures 3a and 3d show that the transversal expansion of the jet, caused by the presence of the obstacle, is very similar to the fixed bed case (Fig. 2b). Independently of the sediment diameter, the bottom erosion (Fig. 3 b and e) is confined close to the original dam location, with relatively small excavation (less than 2 cm). Finally, comparing Figures 3c and 3f, it follows that even the flow momentum is nearly unaffected by the

sediment diameter, showing strong similarities with the fixed-bed counterpart (results not shown for brevity).

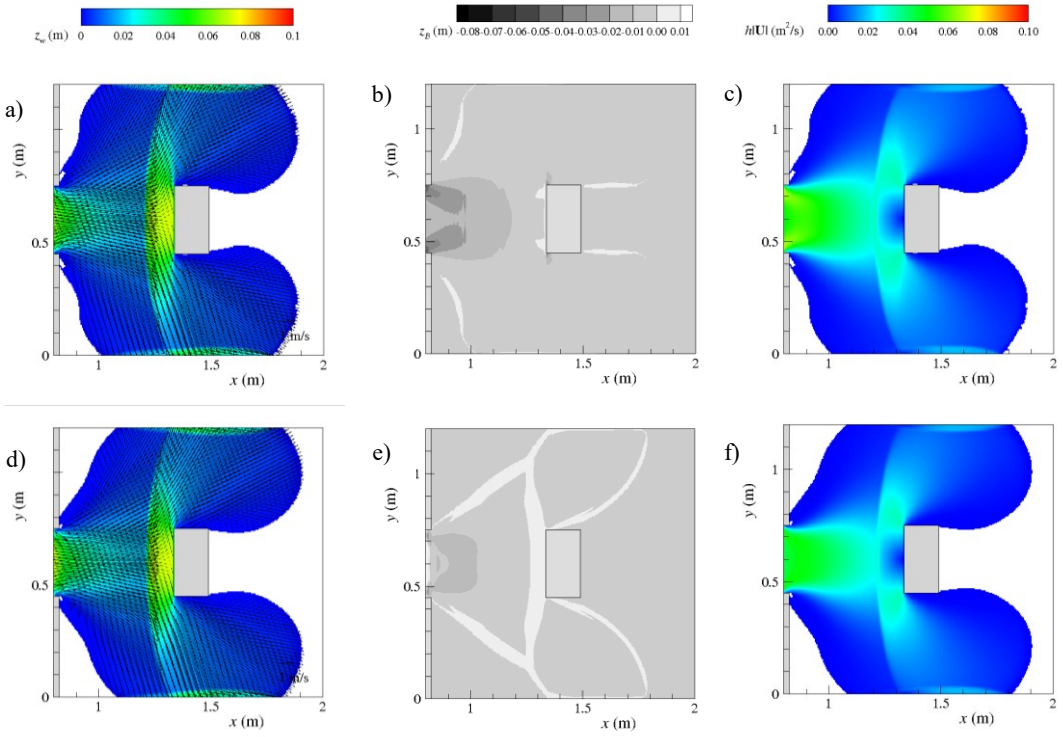

Figure 3: Flow field at t = 1.25 s over mobile bed. Contour levels of the free-surface elevation and velocity vector with $d = 5{\cdot}10^{-4}$ m and $d = 5{\cdot}10^{-3}$ m, a) and d) respectively; of the bottom elevation with $d = 5{\cdot}10^{-4}$ m and $d = 5{\cdot}10^{-3}$ m, b) and e) respectively; of flow momentum with $d = 5{\cdot}10^{-4}$ m and $d = 5{\cdot}10^{-3}$ m, c) and f) respectively.

The above scenario substantially changes at t = 3 s (Figures 4 a-f). Indeed, at this instant, the flood wave reattaches behind the obstacle. Comparing Fig. 2c with Fig. 4a and Fig. 4d, the free surface plots show that the fine sediment promotes the reattachment of the flow, reducing the extension of the wake region compared with the coarse sediment, which indeed behaves more similarly to the fixed-bed case. On the other hand, for the fine sand the flow height in front of the obstacle is substantially lower, which is consistent with the lower values of the impact force (Fig. 2a). Significant differences appear also comparing the bottom topographies (Fig.4 b and e). The fine sediment is characterised by a more pronounced scour hole just downstream the original dam position and at the upstream corners of the obstacle (with depths of about 0.07 cm). Moreover, the bed-forms occurrence, frequent during similar geomorphic transients [25], is detected. These bedforms are far less pronounced with the coarse sediment, which is overall characterised by a less intense morphodynamical change. Finally, comparing the flow momentum distribution (Fig. 4 c and f), it is observed that the interaction with the coarser sediment produces a reduction of the momentum in the region close to the original dam.

4 Conclusions

A numerical study of the propagation of a dam-break wave over an erodible floodplain in the presence of a rigid obstacle has been carried out.

Results have been discussed in terms of flow field modification, bottom deformation and impact force on the obstacle. A literature experiment with non-erodible bed has been considered as test-case. The numerical simulations were carried out by means of a recent shallow-water two-phase model. Results from the numerical simulations contributed to highlight how the presence of the obstacle and the sediment diameter concur to define the final bottom morphology, as well as the role of the bottom erodibility on the time history of the loading condition felt by the obstacle itself. Finally, the capacity of the coarse sediment to reduce the momentum of the flow in proximity of the original dam location has been shown.

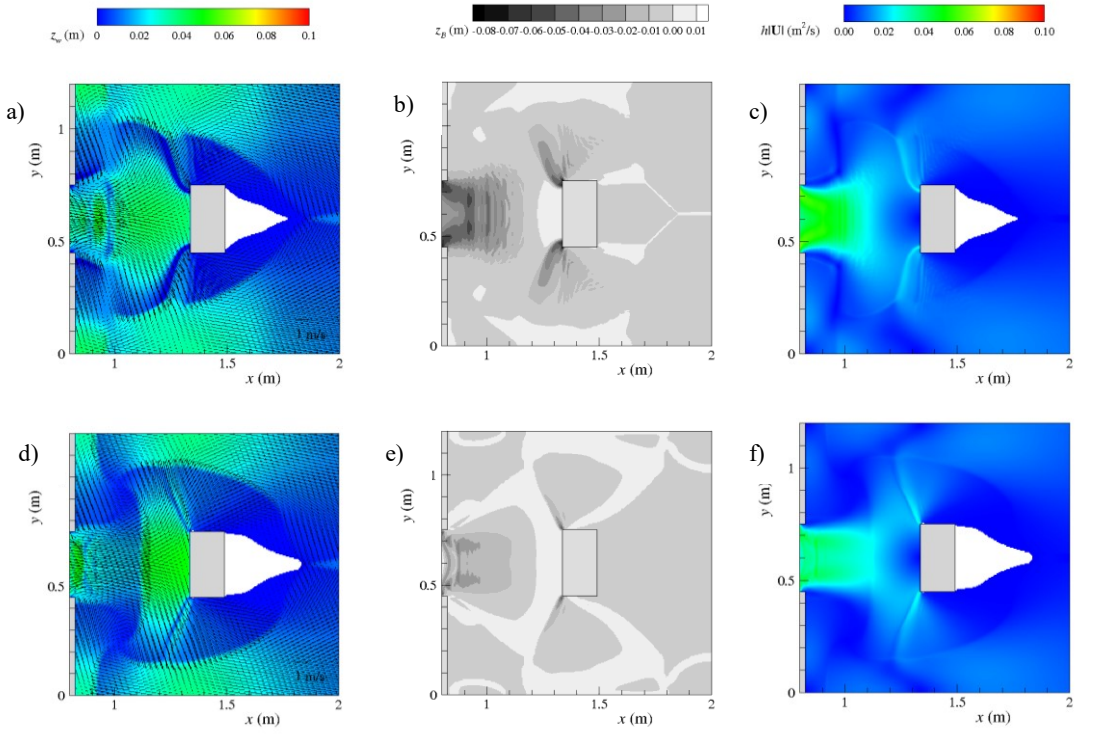

Figure 4: Flow field at $t = 3.0$ s over mobile bed. Contour levels of the free-surface elevation and velocity vector with $d = 5{\cdot}10^{-4}$ m and $d = 5{\cdot}10^{-3}$ m, a) and d) respectively; of the bottom elevation with $d = 5{\cdot}10^{-4}$ m and $d = 5{\cdot}10^{-3}$ m, b) and e) respectively; of flow momentum with $d = 5{\cdot}10^{-4}$ m and $d = 5{\cdot}10^{-3}$ m, c) and f) respectively.

References

[1] M.P. Hoerling, J.W. Hurrell, T. Xu (2001) *Tropical Origin for Recent North Atlantic Climate Change*, Science 292, 90–92.

[2] M. Shige-eda, J.Akiyama (2003) *Numerical and experimental study on two-dimensional flood flows with and without structures*, J. Hydr. Engrg. 129(10), 817–821.

[3] V.I. Bukreev (2009) *Force action of discontinuous waves on a vertical wall*. J. Appl. Mech. Tech. Phys. 50(2), 278–283.

[4] S. Soares-Frazao, Y. Zech (2008) *Dam-break flow through an idealised city*, J. Hydr. Res. 46(5), 648–658.

[5] K. El Kadi Abderrezzak, A. Paquier, E. Mignot (2009) *Modelling flash flood propagation in urban areas using a two-dimensional numerical model*, Nat. Haz. 50, 433–460.

[6] F. Aureli, S. Dazzi, A. Maranzoni, P. Mignosa, R. Vacondio (2015) *Experimental and numerical evaluation of the force due to the impact of a dam-break wave on a structure*, Adv. Wat. Res. 76. 29–42.

[7] A. Palumbo, S. Soares-Frazão, L. Goutiere, D. Pianese, Y. Zech (2008) *Dam-break flow on mobile bed in a channel with a sudden enlargement*, in Proc. of River Flow 2008, 645–654.

[8] S. Soares-Frazão, R. Canelas, Z. Cao, L. Cea, H.M. Chaudhry, A. Die Moran, K. El Kadi, R. Ferreira, I. Fraga Cadórniga, N. Gonzalez-Ramirez, M. Greco, W. Huang, J. Imran, J. Le Coz, R. Marsooli, A. Paquier, G. Pender, M. Pontillo, J. Puertas, B. Spinewine, C. Swartenbroekx, R. Tsubaki, C. Villaret, W. Wu, Z. Yue, Y. Zech (2012) *Dam-break flows over mobile beds: experiments and benchmark tests for numerical models*, J. Hydr. Res. 50(4), 364–375.

[9] W. Wu, S.S.-Y. Wang (2007) *One dimensional modeling of dam break flow over movable beds*, J. Hydr. Engrg. 133(1), 48–58.

[10] Capart, H., & Young, D. (2002). *Two-layer shallow water computations of torrential geomorphic flows*. Proc. of River Flow 2002, Swets & Zeitlinger, Lisse, Netherlands, 1003–1012.

[11] C. Savary, Y. Zech (2007) *Boundary conditions in a two-layer geomorphological model: Application to a hydraulic jump over a mobile bed*, J. Hydr. Res. 45(3),316–332.

[12] C. Swartenbroekx, Y. Zech, S. Soares Frazão (2013) *Two-dimensional two-layer shallow water model for dam break flows with significant bed load transport*, Int. J. Num. Meth. in Fluids 73(5), 477–508.

[13] J. Li., Z. Cao, G. Pender, Q. Liu (2013) *A double layer-averaged model for dam-break flows over mobile bed*, J. of Hydr. Res. 51(5), 518–534.

[14] B. Dewals, F. Rulot, S. Erpicum, P. Archambeau, M. Pirotton (2011) *Advanced topics in sediment transport modelling: Non-alluvial beds and hyperconcentrated flows, sediment transport*. Retrieved from http://www.intechopen.com/books/sediment-transport/advanced-topics-in-sediment-transport-modelling-non-alluvial-beds-and-hyperconcentrated-flows.

[15] M. Greco, M. Iervolino, A. Leopardi, A. Vacca (2012) *A Two-Phase Model for Fast Geomorphic Shallow Flows*, Int. J. Sed. Res. 27(4), 409–420.

[16] G. Rosatti, L. Begnudelli, *A closure-independent Generalized Roe solver for free-surface, two-phase flows over mobile bed* (2013) J. Comp. Phys. 255, 362–383.

[17] C. Di Cristo, M. Greco, M. Iervolino, A. Leopardi, A. Vacca, *Two-Dimensional Two-Phase Depth-Integrated Model for Transients over Mobile Bed* (2016) J. Hydr. Engrg. 142(2) 04015043.

[18] M. Pontillo, L. Schmocker, M. Greco, W.H. Hager (2010) *1D numerical evaluation of dike erosion due to overtopping*, J. Hydr. Res., 48(5), 573–582.

[19] J.F. Richardson, W.N. Zaki, *Sedimentation and fluidisation: Part 1* (1954) Trans. Inst. Chem. Eng. 32, 35–53.

[20] L.C. Van Rijn (1984) *Sediment pick-up functions*, J. Hydr. Engrg. 110(10), 1494–1502.

[21] T.J. Barth, D.C. Jespersen (1989) *The design and application of upwind schemes on unstructured meshes*, AIAA Paper, 89-0366.

[22] A.I. Delis, I.K. Nikolos, M. Kazolea (2011) *An unstructured node-centered finite volume scheme for shallow water flows with wet/dry fronts over complex topography*, Arch. Comput. Meth. Eng. 18,57–118.

[23] A. Harten, P.D. Lax, B. van Leer (1983) *On upstream differencing and Godunov-type schemes for hyperbolic conservation laws*. SIAM Review 25(1), 35–61.

[24] C. Di Cristo, S. Evangelista, M. Greco, M. Iervolino, A. Leopardi, A. Vacca (2017) *Dam-break waves over an erodible embankment: experiments and simulations*, J. Hydr. Res.

[25] B. Spinewine, Y. Zech (2010) *Small-scale laboratory dam-break waves on movable beds*, J. Hydr. Res. 45(sup1), 73–86.